Contents lists available at ScienceDirect

Agricultural Water Management

journal homepage: www.elsevier.com/locate/agwat

Ensemble HYDRUS-2D modeling to improve apparent electrical conductivity sensing of soil salinity under drip irrigation

Theodor Bughici [a,b,*], Todd H. Skaggs [b], Dennis L. Corwin [b], Elia Scudiero [a,b]

[a] University of California, Riverside, Environmental Sciences Department, 900 University Ave., Riverside, CA 92521, USA
[b] USDA-ARS, United States Salinity Laboratory, 50 West Big Springs Rd., Riverside, CA 92507, USA

ARTICLE INFO

Handling Editor: Dr R Thompson

Keywords:
Proximal sensor
Electromagnetic induction
Apparent soil electrical conductivity
Soil salinity mapping
Micro-irrigation

ABSTRACT

Monitoring and mapping soil salinity are valuable for irrigation management and reclamation of salt-affected agricultural soils in arid and semi-arid regions. Proximal measurements of apparent soil electrical conductivity (EC_a) can help characterize soil salinity spatial distributions. However, EC_a is not solely a function of salinity. EC_a is strongly influenced by soil salinity, water content, and edaphic properties such as texture and bulk density. Consequently, monitoring and mapping salinity based on geospatial EC_a measurements is challenging in fields with dynamic and spatially complex patterns of salinity and water content, such as occurs under drip irrigation. We conducted a numerical modeling study to evaluate protocols for using proximal EC_a sensing in drip irrigated systems, focusing specifically on the measurement distance from the drip-line that consistently identifies areas of high salinity in the rootzone. The measurement distance was evaluated as a function of six irrigation management parameters: soil hydraulic conductivity, irrigation discharge, irrigation interval, solute concentration, rootzone volume, and leaching fraction. HYDRUS-2D was used to run a 729 member ensemble of drip irrigation simulations of water and solute dynamics under different irrigation management scenarios. Two case studies were simulated for clay loam soil: (1) low salinity soil irrigated with high salinity irrigation water and (2) high salinity soil irrigated with low salinity water. Depth-averaged EC_a measurements down to the 75 and 150 cm depths, such as can be obtained using an electromagnetic induction (EMI) sensor, were evaluated in the simulations. According to the ensemble results, a reliable EMI measurement distance from the drip-line was about 100 cm for the case of low salinity irrigation in saline soil and adjacent to the drip-line for the high salinity irrigation. The ensemble EC_a and EC of saturated paste extract (EC_e) distributions were twice as sensitive to the irrigation water salinity level as compared to the other irrigation management parameters. The probabilistic ensemble approach can be extended to a variety of case studies to aid soil scientists and agricultural consultants monitoring and mapping soil salinity with EC_a-directed soil sampling for micro-irrigation systems.

1. Introduction

In arid and semi-arid regions, the salt content of soils is a major concern due to its impact on agricultural productivity and sustainability. High levels of soil salinity adversely affect crop growth and yield, soil and water quality, and can ultimately result in soil erosion and land degradation (Rhoades et al., 1990; Corwin and Lesch, 2003). As a major agricultural concern, it is essential to monitor soil salinity at an early stage to effectively use soil resources and maintain soil salinity below the salt stress threshold of crops.

The standard quantitative measure of soil salinity is the electrical conductivity of the saturated soil-water paste extract, EC_e (Corwin and Yemoto, 2020). However, direct measurement of EC_e is time-consuming, labor-intensive, subject to analytical error, and costly. Consequently, for field-scale inventories and monitoring of soil salinity, geophysical methods are usually employed to measure in situ bulk soil electrical conductivity or resistivity, which can be used as a predictor variable to estimate EC_e. One popular geophysical instrument for detecting soil salinity is the electromagnetic induction (EMI) sensor. EMI proximal sensors are easily mobilized and do not require direct contact with the soil, which permits traversing growing crops (Corwin and Lesch, 2005a). EMI sensors provide measurements of depth-weighted apparent bulk electrical conductivity (EC_a). Typically, readings are taken with the instrument in horizontal (EM_h) and vertical (EM_v) dipole orientations,

* Corresponding author at: University of California, Riverside, Environmental Sciences Department, 900 University Ave., Riverside, CA 92521, USA.
E-mail address: theodorb@ucr.edu (T. Bughici).

https://doi.org/10.1016/j.agwat.2022.107813
Received 2 December 2021; Received in revised form 27 June 2022; Accepted 3 July 2022
Available online 20 July 2022

providing two depth-averaged measurements of EC_a with differing depth-weighted response functions. Field EC_a is influenced by multiple soil factors including soil salinity, clay content, cation exchange capacity, clay mineralogy, soil pore size distribution, soil water content (θ), and temperature, as well as the depth response function of the sensor (Rhoades et al., 1989; Corwin and Lesch, 2005a). Williams and Baker (1982) observed that in salt-affected soils, 65 % of the variation in measurements could be explained by soluble salt concentration alone. In non-saline soils, conductivity variations are primarily a function of soil moisture content, texture, and cation exchange capacity (CEC). Pedrera-Parrilla et al. (2016) found that the correlation between EC_a and clay content was twice as high under wet soil conditions as compared to dry.

The multiplicity of factors potentially affecting EC_a complicates its use as a predictor variable for EC_e. Protocols and guidelines for geophysical surveys and data analyses have been developed to aid in determining EC_e (Corwin and Lesch, 2003, 2005b, 2013). Corwin and Scudiero (2020) summarized the protocols. Recommendations include performing geophysical surveys relatively soon after rainfall or irrigation such that homogeneity of field soil moisture is maximized, and using EC_a directed soil sampling to develop site-specific EC_e regression equations requiring a relatively small number of soils samples (Lesch et al., 1995; Corwin and Lesch, 2005b).

The early EC_a-directed soil sampling protocols and guidelines developed by Corwin and Lesch (2003), (2005b) were devised for natural precipitation and flood and sprinkler irrigation systems where local-scale variation in soil salinity is less complex than micro-irrigation systems since water infiltrating at the soil surface is relatively uniform in comparison. Subsequently, Corwin and Lesch (2013) developed EC_a-directed soil sampling protocols for fields under drip irrigation, which involved taking two separate EC_a surveys, one along the drip line and one between drip lines to characterize the dramatically different soil moisture and salinity regimes that existed in the drip lines and between the drip lines. However, as shown by Corwin et al. (2022) these EC_a-directed soil sampling protocols and guidelines were inadequate for mapping the complex local-scale 3-dimensional nature of salinity resulting from well-established micro-irrigation systems (i.e., drip, buried drip, micro sprinklers, etc.) in use for a decade or longer. When following the EC_a-directed soil sampling protocols of Corwin and Lesch (2013) to map field-scale soil salinity for a field under drip irrigation, a single soil core is taken at the location of a drip emitter for selected locations within the field determined from model- (e.g., response surface sample design) or design-based (e.g., stratified random sampling) sample designs based on the spatial variability of EC_a measurements. The soil sample is in the "sweet" spot (i.e., the location where the salinity is leached the most and is the lowest), which is not representative of the 1–2 m^2 volume of measurement of the electromagnetic conductivity meter (i.e., Geonics EM38) used to measure EC_a. The induced electromagnetic field encompasses the full salinity gradient created by the drip emitter, resulting in EC_a measurements (i.e., measurement of EC_a in the horizontal coil configuration, EM_h, and in the vertical coil configuration, EM_v) that are not representative of the salinity in the soil core taken directly below the drip emitter. Subsequently, the electrical conductivity of the saturation extract (EC_e) obtained from the soil core sample is not representative, resulting in an erroneous EC_a to EC_e calibration (Corwin et al., 2022). To map soil salinity accurately for fields under drip irrigation Corwin et al. (2022) developed a modified set of protocols for mature drip-irrigation systems that accounts for the complex local-scale variability in salinity around drip lines. An essential part of the EC_a-directed soil sampling protocols for drip irrigation systems involves the determination of the location of the EMI measurement and soil core location that will provide the best EC_a–EC_e calibration around the drip line. Corwin et al. (2022) recommended the use of transient solute transport models such as HYDRUS-2D to establish the location of EMI measurements and soil core samples to create the best EC_a–EC_e calibration, thereby eliminating the need for labor and cost-intensive soil cores and their analysis for each crop and set of soil conditions.

It is the object of this paper to demonstrate and evaluate the use of a transient solute transport model to determine the optimal EMI measurement and soil core location from the drip line for calibrating EC_a to EC_e from geospatial EMI measurements for a field under drip irrigation. The determination of the optimal EMI measurement and soil core locations to best calibrate EC_a to EC_e for various crops and soil conditions is a crucial tool to map and monitor the complex local- and field-scale variation in soil salinity for drip irrigation systems using EC_a-directed soil sampling (Corwin et al., 2022).

2. Methods

We use HYDRUS-2D simulations to investigate optimal positioning for EMI measurements and ground-truth soil cores. The goal is to obtain field measurements that identify high EC areas and reduce the uncertainty in field observations. An ensemble of 729 simulations is used to account for uncertainty in the input parameters and boundary conditions. The workflow for the ensemble simulation is outlined in Fig. 1 and detailed below. As a demonstration, we consider two case studies for drip-irrigated orchards, also explained below.

2.1. Numerical modeling

Drip irrigation simulations were done using the HYDRUS-2D software. HYDRUS-2D uses a Galerkin finite-element method based on the mass conservative formulation proposed by Celia et al. (1990). Flow individual emitters can be considered axisymmetric until the wetting patterns from neighboring emitters begin overlapping. After that, the axisymmetric representation can only be an approximation of the fully three-dimensional problem (Kandelous et al., 2011). Although drip irrigation typically consists of many emitters with overlapping wetted soil volumes, in our simulations we considered axisymmetric flow from a single emitter assuming negligible overlap. The Richards equation governing axisymmetric water flow in homogeneous and isotropic soil is:

$$\frac{\partial \theta(h)}{\partial t} = \frac{1}{r}\frac{\partial}{\partial r}\left[r\,K(h)\frac{\partial h}{\partial r}\right] + \frac{\partial}{\partial z}\left[K(h)\frac{\partial h}{\partial z} + K(h)\right] - S(h) \quad (1)$$

where θ is the volumetric soil water content (L^3L^{-3}), h is the soil water pressure head (L), t is time (T), r is the radial coordinate (L), z is the vertical space coordinate (L), K is the hydraulic conductivity (LT^{-1}), and

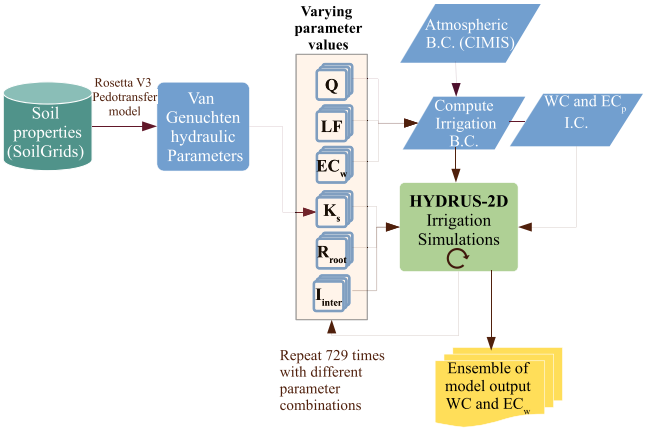

Fig. 1. Flow-chart of the ensemble modeling setup using HYDRUS-2D. Q is emitter discharge, LF is irrigation leaching fraction, K_s is soil saturated hydraulic conductivity, R_{root} is the radius of the root system, I_{inter} is the irrigation interval, B.C. is model boundary conditions, I.C. is model initial conditions, WC is soil water content, and EC_p EC_w are the electrical conductivity of the soil pore water and of the irrigation water, respectively.

S is the sink term accounting for water uptake by plant roots ($L^3L^{-3}T^{-1}$). The unsaturated soil hydraulic properties were described using the van Genuchten-Mualem functional relationships (Van Genuchten, 1980):

$$S_e(h) = \frac{\theta(h) - \theta_r}{\theta_s - \theta_r} = \frac{1}{(1 + |\alpha\, h|^n)^m} \tag{2}$$

$$K(h) = K_s\, S_e^{0.5}\left[1 - (1 - S_e^{1/m})^m\right]^2 \tag{3}$$

in which S_e is the effective saturation; θ_r and θ_s are the residual and saturated water contents (L^3L^{-3}), respectively; K_s is the saturated hydraulic conductivity (LT^{-1}); and α (L^{-1}), m, and n are shape parameters with $m = 1 - 1/n$.

Solute transport in a homogeneous, axisymmetric domain was computed using the convection-dispersion equations (CDE):

$$\frac{\partial \theta C}{\partial t} = \frac{1}{r}\frac{\partial}{\partial r}\left[r\left(\theta D_{rr}\frac{\partial C}{\partial r} + \theta D_{rz}\frac{\partial C}{\partial z} - q_r C\right)\right] - \left[\theta D_{zz}\frac{\partial C}{\partial z} + \theta D_{rz}\frac{\partial C}{\partial z}\right] - S(h)C_s \tag{4}$$

where C is the total solute concentration (ML^{-3}); C_s is the concentration of the water extracted by roots (ML^{-3}); q_r and q_z are the radial and vertical volumetric fluid fluxes (LT^{-1}), respectively; and D_{rr}, D_{rz}, D_{zz}, and D_{rz} (L^2T^{-1}) are dispersion coefficients that were modeled as functions of solute velocities and dispersivities using standard equations (Bear, 2013). Longitudinal and transverse dispersivities were set to 0.5 and 0.1 cm, respectively. Equation 4 neglects chemical reactions and interactions with the solid phase.

We assume relatively low solute concentrations such that the electrical conductivity of a solution is proportional to its total solute concentration. The proportionality permits directly replacing units of concentration in Eq. 4 with units of electrical conductivity, dS m^{-1}. The solute is taken up passively by roots until a threshold concentration, $C_{s,max}$, is reached (Šimunek and Hopmans, 2009); we set the threshold to 1 dS m^{-1}. The Feddes root water uptake stress parameters (Feddes and Zaradny, 1978) were based on values given for orange trees (Grieve et al., 2012) in the HYDRUS-2D software, since no data is available for Pistachio trees in the literature.

Except in very coarse-textured soils, water from surface drip emitters often travels a short distance overland before infiltrating. Thus, rather than a point source, the surface emitter was represented as a 10 cm radius source (Fig. 2). The domain size was 300 × 300 cm with free drainage at the bottom boundary (Fig. 2).

2.2. Apparent bulk soil electrical conductivity

Three main pathways exist for electrical conduction in soils: via soil water occupying the larger pores; via cations on exchange surfaces; and via solid particles in direct and continuous contact with one another (Rhoades et al., 1999). In sufficiently moist soils, the dominant pathway is via the soil pore solution. Rhoades et al. (1989) formulated a model for the apparent bulk soil electrical conductivity (EC_a) that integrates the conductivities of the three pathways:

$$EC_a = \left[\frac{(\theta_{SS} + \theta_{WS})^2 EC_{WS} EC_{SS}}{\theta_{SS} EC_{WS} + \theta_{WS} EC_S}\right] + (\theta_W - \theta_{WS}) EC_{WC} \tag{5}$$

where θ_{WS} and θ_{WC} are the volumetric soil water contents in the soil water and continuous liquid pathways ($cm^3\ cm^{-3}$), respectively; θ_{SS} and θ_{SC} are the volumetric contents of the surface-conductance and solid phases ($cm^3\ cm^{-3}$), respectively; EC_{WS} and EC_{WC} are the conductivities of the soil water pathway and continuous liquid pathway (dS m^{-1}), respectively; and EC_{SS} and EC_{SC} are the conductivities of the surface-conductance and solid phases (dS m^{-1}), respectively.

With knowledge of soil bulk density and assuming uniform clay and organic matter contents and the soil not being extremely dry (Corwin and Lesch, 2005a), it is possible to express the constituent conductivities as functions of soil properties and degree of water saturation, and thus relate EC_a to θ and the pore water EC (EC_p). We assume $\theta = \theta_{WS} + \theta_{WC}$ = total volumetric water content ($cm^3\ cm^{-3}$). The following empirical approximations have been evaluated by Corwin and Lesch (2003) and Farahani et al. (2005):

$$\theta = \frac{P_W\, d_b}{100} \tag{6}$$

$$\theta_{WS} = 0.639\,\theta_W + 0.011 \tag{7}$$

$$\theta_{SS} = \frac{d_b}{2.65} \tag{8}$$

$$EC_{SS} = 0.19\, S_e - 0.434 \tag{9}$$

$$EC_W = \left[\frac{EC_e\, d_b\, S_e}{100\,\theta_w}\right] \tag{10}$$

$$EC_{SS} = -2.1 + 2.3\, CP \tag{11}$$

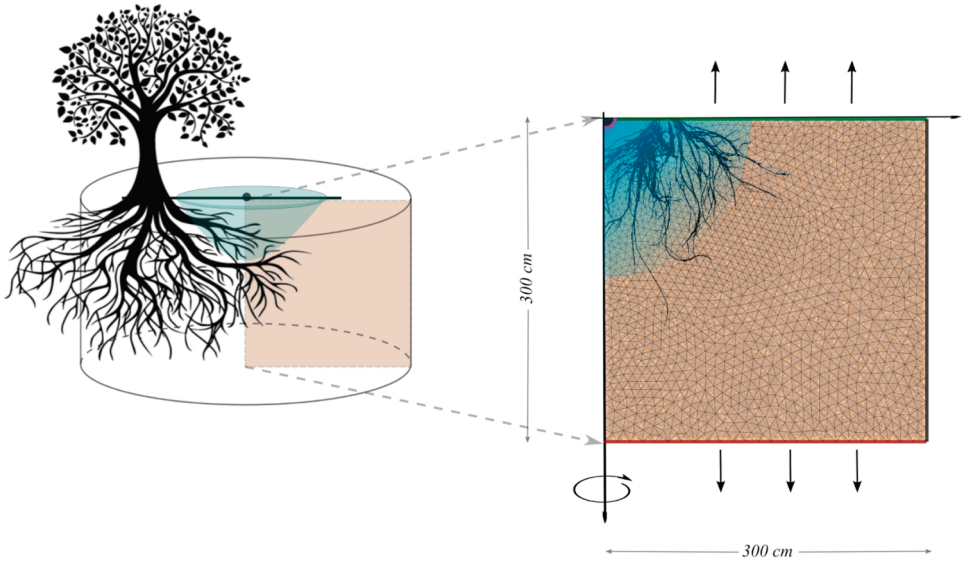

Fig. 2. The 300 × 300 cm axisymmetric domain and finite element mesh used to simulate water flow, solute transport, and root water uptake beneath a single emitter.

where P_W is the gravimetric water percentage, d_b is the bulk density (Mg m^{-3}), EC_W is the average electrical conductivity of the saturated extract (dS m^{-1}), and CP is clay percentage. Fig. 3 shows the $\theta - EC_a - EC_p$ relationship for the clay loam soil used in this study (discussed below). Fig. 4.

To simulate EMI measurements, we suppose an EMI sensor is located at the surface of the axisymmetric domain a distance r from the emitter. Measurements taken in the vertical (EM_v) and horizontal (EM_h) configurations average the simulated bulk soil EC directly beneath the sensor down to the 75 and 150 cm depths, respectively. Note that concerning the axisymmetric domain, moving the sensor along a path parallel to the drip line and moving the sensor on a path perpendicular to an emitter are comparable in terms of increasing the distance r from the emitter (Fig. 5a).

2.3. Case studies and model ensemble

Two case studies were developed featuring either a high or low initial soil salinity. Soil parameters and surface boundary conditions were based on conditions found in Flores commercial pistachio orchards near Lemoore, CA (36.192°*N*, 129.881°*W*), a highly productive agricultural area in the Central Valley of California that is home to a variety of tree crops. Soils in the region often have high salinity due to combinations of some or all of the following: irrigation, poor drainage, high water tables, high levels of evapotranspiration, and high levels of naturally occurring salts.

The soil was taken to be homogeneous with characteristics based on the soil found in the Flores pistachio orchard. From the SoilGrids database (Hengl et al., 2017, representative soil properties for the clay loam soil were determined to be 36 % sand, 37 % silt, 27 % clay, and bulk density equal to 1.59 g cm^{-3}. The Rosetta V3 pedotransfer function (Zhang and Schaap, 2017 was used to estimate soil hydraulic parameters from the soil properties. The resulting parameters were $\theta_r = 0.103$; $\theta_s = 0.412$; $\alpha = 0.0071$; cm^{-1}; $n = 1.37$; and $K_s = 0.363$ cm h^{-1}).

The model runs for the case studies simulated 60 days, with surface boundary conditions reminiscent of early season (April-May) pistachio irrigation. Crop potential evapotranspiration was calculated based on the Penman-Monteith equation (Allen et al., 1998 using hourly meteorological data from CIMIS (California Irrigation Management Information System) station no. 80. The crop coefficient (K_c) for April and May were 0.25 and 0.75, respectively (based on Goldhamer, 2005). The 60-day simulation was found to be sufficient for wetting of the entire root zone. The simulations ran with uniform initial θ (70 % of field capacity) and pore water salinity, $EC_{p,init}$ (values used for case studies discussed below). Potential crop evapotranspiration (ET_c) and water

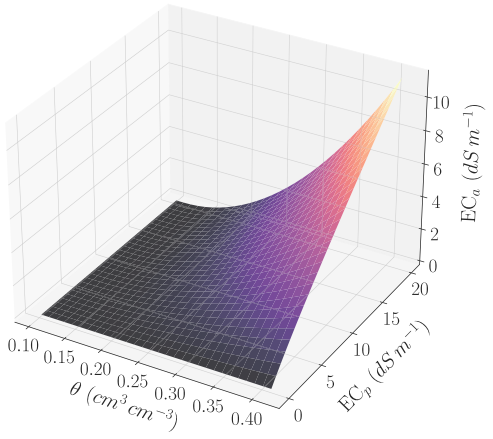

Fig. 3. Plot of EC_a as a function of soil water content (θ) and pore water EC (EC_p) for the clay loam soil used in this study, according the formulation of Rhoades et al. (1989) (Eq. 5).

requirements per tree assumed one tree per 48 m^2 and 8 emitters per tree. Applied irrigation water was determined according to $ET_c + ET_c \times LF$, where LF is the target leaching fraction, ET_c was calculated according to a theoretical perfect forecast from one irrigation to the next, and the evaporation fraction was assumed to be 0.15 (based on similar evaporation-transpiration partitioning in drip-irrigated tree crops, Kool et al., 2014).

One case study featured an initial low pore water EC ($EC_{p,init}$ = 1 dS m^{-1}) irrigated with higher EC_w, and the other a high $EC_{p,init}$ (= 12 dS m^{-1}) and lower EC_w irrigation water. To account for uncertainty or variability in system parameters, simulation runs were made using combinations of three possible values for six selected model parameters, giving a total of $3^6 = 729$ combinations and simulations for each case (Table 1). The model parameters were selected based on their high impact on solute distribution in drip irrigation (Mmolawa and Or, 2000). The selected parameter values for initial pore water EC ($EC_{p,init}$), irrigation water EC (EC_w), emitter discharge (Q), leaching fraction (LF) and irrigation interval (I_{inter}) are within the range of common drip irrigation practices that are also applied in Pistachio orchard irrigation in our study area (Dasberg and Or, 1999; Burt and Isbell, 2005; Mehdi-Tounsi et al., 2017). Pistachio root-zone radius (R_{root}) range was based on the Pistachio effective root-zone depth that is often considered in the study area (Baram et al., 2016; Burt et al., 2003) and soil saturated hydraulic conductivity (K_s) range was ± 20% of the calculated value, maintaining it in a range typical of a clay loam soil.

EC_a and EC_e are presented as normalized values (noted as $\widetilde{EC}_a$ and $\widetilde{EC}_e$, respectively). The normalization is calculated by dividing each value of the grid element by the sum in the domain and weighted by the element size. The normalization is done to facilitate comparisons between ensemble members differing in water content and applied solute. To estimate the relative importance of each variable in Table 1, a simple sensitivity analysis was performed. For each parameter, the coefficient of variation (CV) of the final simulated normalized apparent bulk soil EC ($\widetilde{EC}_a$) was calculated for the subset of model runs made while setting that the parameter to its middle value (Table 1). Among the calculated CVs, a relatively low value obtained for a given parameter would indicate the parameter, when not held fixed, had a relatively high impact on the model output variance.

2.4. Ensemble analysis

Of interest is the correlation between water content and soil salinity to the apparent EC (EC_a). If EC_e is not correlated to EC_a, it will be difficult to reliably infer salinity levels from measured EC_a values. The EC_e–EC_a and θ–EC_a correlations were calculated for 5 cm horizontal radius increments, down to 75 cm (EMI_v measurement configuration) and to 150 cm (EMI_h) configuration. A rolling window Pearson correlation coefficient (ρ) was calculated between the vertical means of EC_e and EC_a as well as between θ and EC_a. EC_e was taken to be the soil water EC at saturation. To clarify that correlations do not change significantly with time during and between irrigations, the rolling correlation was calculated for all ensemble members of both cases and the ensemble mean was compared between the last 16 output times of the last 72 h of simulation, using an index of agreement (Willmott, 1981) as a standardized measure of model prediction error (varies between 0 and 1).

The EC_a and EC_e values were also calculated based on the mean value obtained when EMI measurements traversed parallel to the dripline at a distance d, thus averaging a soil area of changing horizontal radii from the emitter (Fig. 5). This calculation provides the theoretical EC_a values measured in the modeled field and compared to the simulated EC_e values.

2.5. Field data

Qualitative comparisons between simulations and field data were

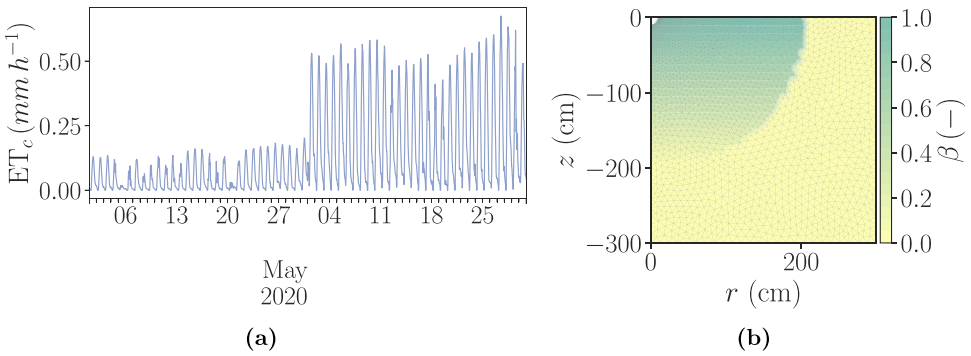

Fig. 4. Boundary conditions and root distribution generated for the irrigation simulations:(a) Potential crop evapotranspiration (ET_c) used as boundary conditions in the simulations and (b) spatial root density distribution (β). The generated root-zone was spherical with β decreasing linearly with depth.

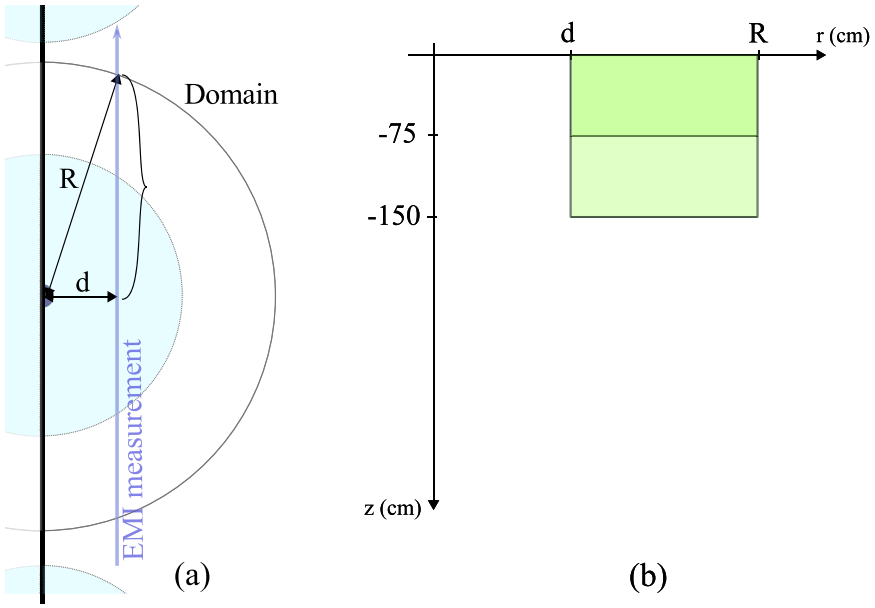

Fig. 5. (a) Overhead view of the EMI measurement path at a distance d from the drip-line and (b) the soil area sensed moving the sensor from a distance $r = d$ to $r = R$ in either the vertical (75 cm) or horizontal configuration (150 cm).

Table 1
Parameter values used to generate ensembles of $3^6 = 729$ simulations for the high and low $EC_{p,init}$ case studies. $EC_{p,init}$ = initial pore water EC; EC_w = irrigation water EC; Q = emitter discharge; LF = leaching fraction; I_{inter} = irrigation interval; R_{root} = root-zone radius; K_s = soil saturated hydraulic conductivity.

Parameter	Low $EC_{p,init}$	High $EC_{p,init}$
$EC_{p,init}$ (dS m^{-1})	1	12
EC_w (dS m^{-1})	[3, 5, 8]	[1, 3, 5]
LF (–)	[0.05, 0.1, 0.15]	
Q (L h^{-1})	[3, 4, 5]	
I_{inter} (h)	[48, 72, 96]	
R_{root} (cm)	[100, 150, 200]	
K_s (cm h^{-1})	[0.290, 0.363, 0.435]	

made. Two subsections within the Flores pistachio orchard in Lemoore, CA designated D01 and D05 were selected to provide relevant soil data. Subsection D01 was 230 × 200 m and D05 was 200 × 200 m. Soil sample sites were selected using the EC_a-directed soil sampling protocols summarized by Corwin and Scudiero (2020) to provide a range of variation in soil properties. The details of the EC_a survey and soil sampling can be found in the associated paper by Corwin et al. (2022). A brief overview of the EC_a survey and soil sampling will be provided for orientation.

Geospatial surveys of EC_a for D01 and D05 were conducted using a mobile cart pulled by hand with electromagnetic induction (EMI) and coupled GPS equipment secured to the cart. Ten equally spaced traverses (20 m apart) were taken with the electromagnetic conductivity meter within each of the Flores (D01 and D05) sites. Along each traverse, EC_a measurements were taken every 3–5 m. Measurements of EC_a were taken in the horizontal (EM_h) and vertical (EM_v) dipole modes to provide shallow (0–0.75 m) and deep (0–1.5 m) measurements of EC_a, respectively.

Using the EC_a survey data, 6 sampling locations were selected at each site (i.e., Flores D01 and Flores D05) to represent the frequency distribution of the bivariate EMI survey data for each site, and to be allocated across each site to avoid spatial clustering. Soil cores were taken at 6 locations within both D01 and D05. At each of the 12 locations (6 locations for D01 and 6 locations for D05) soil cores were taken at 0, 0.3, 0.6, 0.9, 1.2, and 1.5 m perpendicular to the drip line at 0.3-m depth increments down to 1.5 m. The cores taken at 0, 0.3, 0.6, 0.9, 1.2, and 1.5 m perpendicular to the drip line were used to characterize the salinity gradients created by drip irrigation. All soil cores were kept in refrigerated storage before air-drying and sieving (2-mm sieve), which occurred within a few days after their collection. Soil samples were analyzed for electrical conductivity of the saturated paste extract (EC_e),

saturation percentage (SP), Sodium adsorption ratio (SAR), gravimetric water content at field capacity (θ_g), and pH of the saturated paste extract following the chemical analysis procedures presented by Rhoades (1996). SAR was estimated after determining Ca, Mg, and Na concentrations in the saturated paste extract. The field EC_e and θ measured values are qualitatively compared to the model results.

3. Results and discussion

3.1. Simulation results and field data

Example results for one of the simulated soil profiles obtained at the end of the 60-day simulation are shown in Fig. 6. The patterns and trends shown were roughly the same for all 729 realizations. The water content (presented as saturation degree normalized to field capacity, $S_e/S_{e,\,FC}$) has the same pattern for both case studies (left panels in Figs. 6a and 6b). There is some difference in S_e between cases at the edge of the wetted bulb, at about 150–180 cm from the dripper. The wetter soil in the high $EC_{p,init}$ case are caused by relatively less water uptake occurring in areas of the root zone with higher salinity (Fig. 6b, right panel). The salinity profiles differ between cases (Figs. 6a vs 6b, right panels). The low $EC_{p,init}$ case has a higher concentration of salinity close to the dripper, as most salts in the profile were added with the irrigation water and accumulated in the rootzone. The high $EC_{p,init}$ case has lower EC_e close to the dripper while the salts being leached by relatively low EC water accumulate at the periphery of the wetted bulb. The two case studies represent possible scenarios where present irrigation water quality differs from that used in the past.

At both sites sampled in the Pistachio orchard, EC_e was positively correlated with distance from the emitter (Fig. 7). At site D01, the EC_e vs. distance correlation was $R^2 = 0.32$ when calculated for all transects at the site (Fig. 7b). At site Do5, the correlation was $R^2 = 0.49$ (Fig. 7c). The measured EC_e values have a qualitative resemblance to the high $EC_{p,init}$ case results, with a general increasing EC_e gradient when moving away from the emitter and with a similar range of EC_e values presented in Fig. 6a.

The field data and modeled high $EC_{p,init}$ case study represent saline soils irrigated with relatively good quality water and thus solute concentration gradients are positive moving away from the emitter.

3.2. Ensemble analysis

3.2.1. θ-EC_a correlation and EC_e-EC_a correlations

In the low $EC_{p,init}$ case, θ-EC_a and EC_e-EC_a correlations for simulated EM_v measurements (150 cm averaging depth) are positively high out to a radial distance of 100 cm from the emitter for all three presented simulation times, with small variance between ensemble members (Fig. 8a,c,e). The EM_h results (75 cm averaging depth) show a lower (mostly positive) correlation and higher variance over the same radial distance. For the high $EC_{p,init}$ case, θ-EC_a and EC_e-EC_a correlations are lower (sometimes negative) over the 0–100 cm distance as compared to the low $EC_{p,init}$ case. In most of the wetted area (radial distance 0–120 cm), the θ-EC_a correlation for the high $EC_{p,init}$ case is negative for EM_v, and is low with large ensemble variability for EM_h (Fig. 8d,f). This is caused by the general positive EC_e gradient and a negative θ gradient with distance from the emitter (Fig. 6b).

For both measurement depths at the end of the simulations, there is an area of high positive θ-EC_a and EC_e-EC_a correlation at 80–150 cm distance in the low $EC_{p,init}$ case (Fig. 8c,e), and at 130–180 cm in the high $EC_{p,init}$ case (Fig. 8d,f). This range of distances away from the

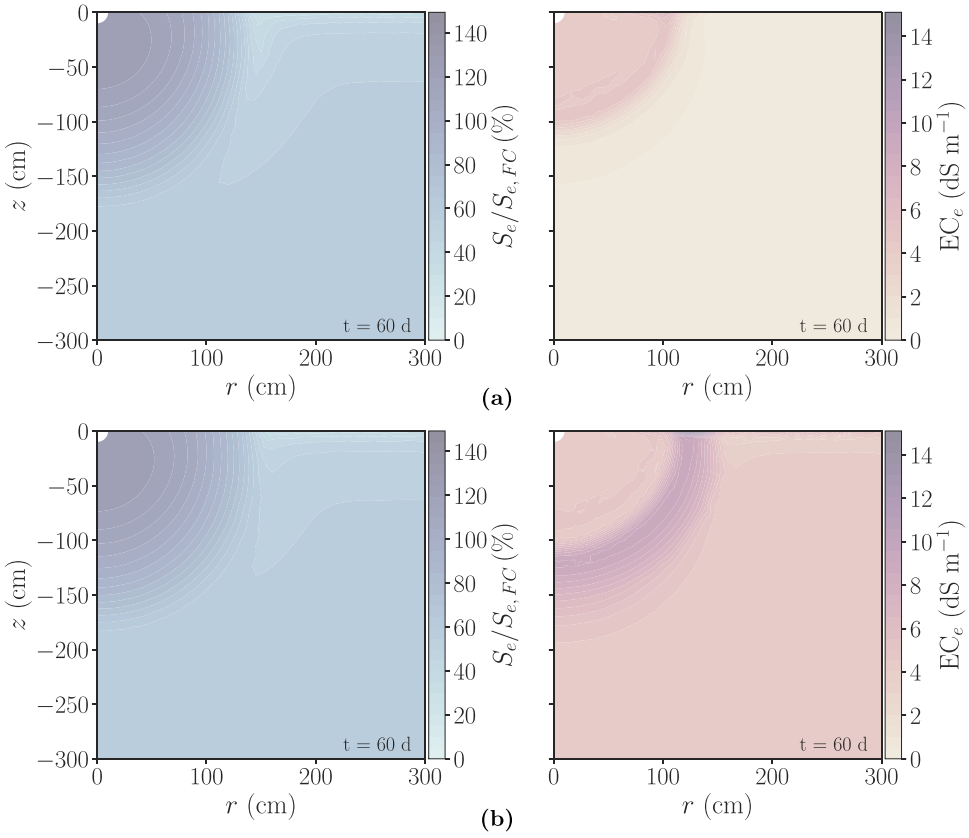

Fig. 6. Example normalized field capacity saturation degree ($S_e/S_{e,\,FC}$, left panels) and saturated paste extract electrical conductivity (EC_e, right panels) obtained at the end of one of the 729 simulations for the (a) low and (b) high $EC_{p,init}$ case studies. In the plots, z is depth and r is distance from emitter. Simulation parameters for this example were: $Q = 4$ L h^{-1}, $LF = 0.1$, $K_s = 0.363$ cm h^{-1}, $R_{root} = 150$ cm, $I_{inter} = 72$ h, and $EC_w = 5$ dS m^{-1} for the low case (a) and $EC_w = 3$ dS m^{-1} for the high (b).

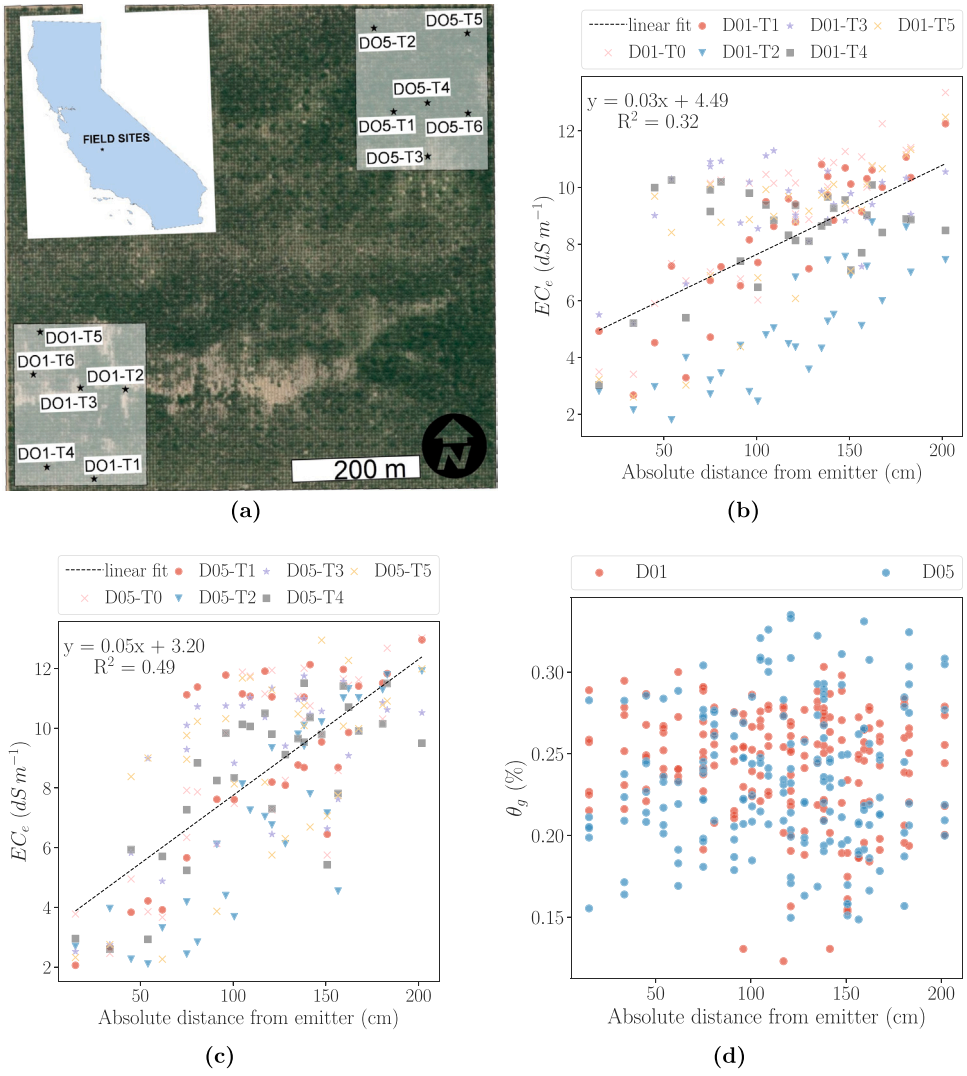

Fig. 7. The location of two Pistachio sites and each soil sampling transect (a), The Saturated paste extract electrical conductivity (EC_e) for each transect with correlation to distance from the emitter at each site (b-c) and gravimetric water content (θ_g) for both sites (d). The linear fit of EC_e vs. absolute distance from the emitter is plotted for each transect and also the overall fit and correlation (R^2) calculated for all transects in each site (dashed black lines).

dripper can be considered a reliable distance for EC_a measurements since EC_e-EC_a are highly correlated with a small variability between ensemble members (Fig. 8b,c,d,e). The EC_e-EC_a correlation was generally greater (more positive) and more reliable (smaller variance) for the 150 cm measurement depth than for the 75 cm depth.

The index of agreement of mean correlations of θ-EC_a and EC_e-EC_a in the last 72 h of simulations (16 in total) was higher than 0.96 by average for all cases and depths. The high agreement indicates the correlations presented in Fig. 8 do not change drastically in the later stages of the simulations.

3.2.2. Calculated ensemble EC_a and sensitivity analysis

To further understand θ and EC_e dynamics and their potential effect on EC_a measurements with an EMI device, it is important to consider the entire EC_a soil profile. The mean and CV of the calculated $\widetilde{EC}_a$ (Eq. 5) of the ensemble members were computed at the end of the simulations (Fig. 9). The low $EC_{p,init}$ case has the higher averaged $\widetilde{EC}_a$ very close to the emitter where both moisture and solute concentrations are high (Fig. 9a). For the high $EC_{p,init}$ case, the displaced salts are concentrated towards the edges of the wet area and increase the $\widetilde{EC}_a$ at that area despite it being drier (as shown for one ensemble member in Fig. 6). For the high $EC_{p,init}$ case, proximal measurement far from the wetted bulb may be misleading since there is a high $\widetilde{EC}_a$, but high salinity in those areas might not have influence on the root-zone and thus the tree health and production (Fig. 9b).

For both cases there is higher ensemble variability in $\widetilde{EC}_a$ toward the edges of the wet bulb (Fig. 9) but the low $EC_{p,init}$ case has a low variability close to the emitter and the high $EC_{p,init}$ case has a also high variability close to the emitter. Thus, for the low $EC_{p,init}$ case, the higher relative concentration of soil EC_a is close to the dripper with low variability, making it the ideal area for measurements, but for the high $EC_{p,init}$ case the area of high $\widetilde{EC}_a$ is also characterized by high ensemble variability implying the $\widetilde{EC}_a$ in this area will differ depending on irrigation management (Fig. 9).

The sensitivity analysis that measured the ensemble CV of $\widetilde{EC}_a$ when each parameter is held fixed shows the largest contribution to ensemble variance was by EC_w for both case studies (Fig. 10). The I_{inter} parameter was the second largest contributor to ensemble uncertainty in both case studies. The contribution of all other parameters was similar. For this case study knowledge of irrigation water salinity level may be of high benefit in assessing optimal locations for proximal salinity sensing. Other case studies, with different ranges of parameters, may give different results since any sensitivity analysis is largely dependent on the parameter range. Prior knowledge of this range of possible values can

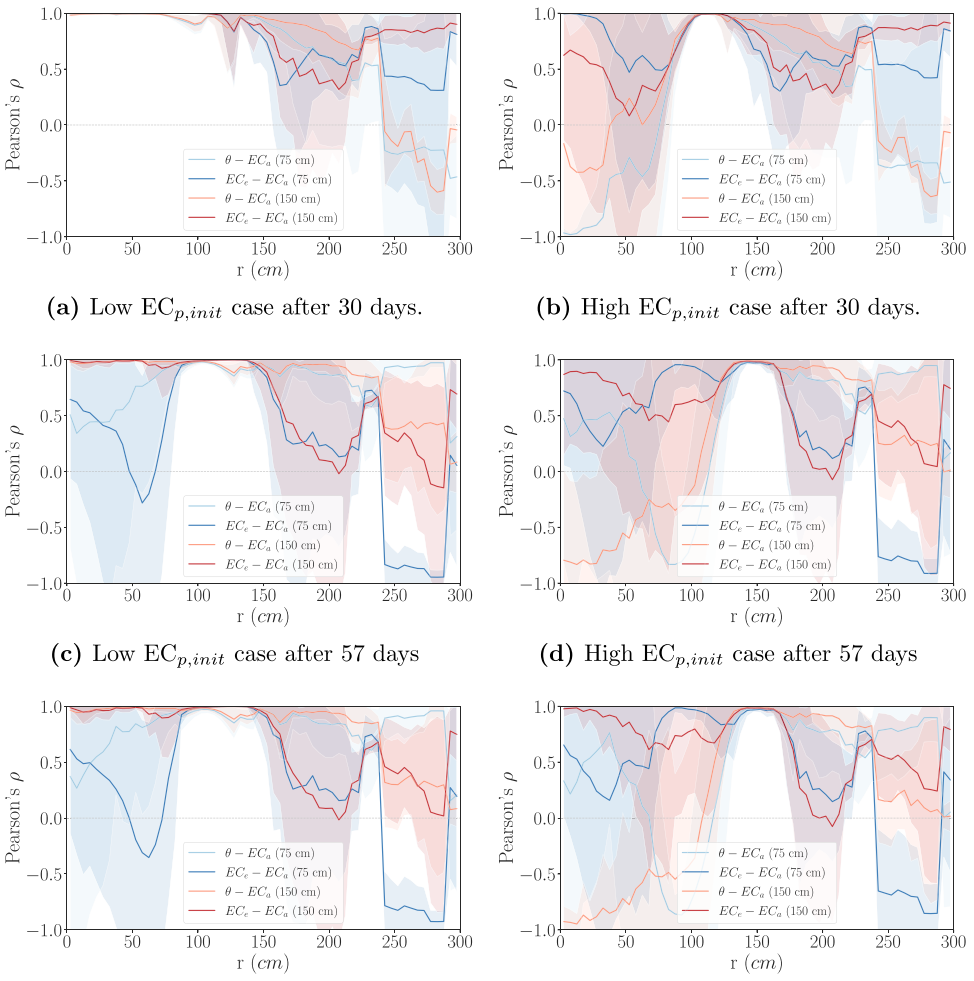

(a) Low $EC_{p,init}$ case after 30 days. (b) High $EC_{p,init}$ case after 30 days.

(c) Low $EC_{p,init}$ case after 57 days (d) High $EC_{p,init}$ case after 57 days

(e) Low $EC_{p,init}$ case after 60 days (f) High $EC_{p,init}$ case after 60 days

Fig. 8. Rolling Pearson correlation between soil volumetric water content and apparent electrical conductivity (θ–EC_a) and between saturated paste extract electrical conductivity and apparent electrical conductivity (EC_e–EC_a)) after 30, 57, and 60 days of simulation (a-b, c-d, e-f, respectively). The depths over which θ and EC_e have been averaged correspond to horizontal (EM_h, 0–75 cm) and vertical (EM_v, 0–150 cm) configurations of the EMI instrument. Lines indicate the mean ensemble value and shaded regions show plus-or-minus two ensemble standard deviations. Both case studies are presented, initial low soil water EC irrigated with high EC water (Low $EC_{p,init}$, panels a,c,e) and Initial high soil water EC irrigated with low EC water (High $EC_{p,init}$, panels b,d,f).

help reduce uncertainty when applying this modeling framework to other case studies.

3.2.3. EC_a with distance from the drip-line

When calculating $\widetilde{EC}_a$ and $\widetilde{EC}_e$ along a parallel path at a distance d from the drip-line, average values decrease with increasing d, and then remain low and close to constant after 120 cm for the low $EC_{p,init}$ case (Fig. 11a). For the high $EC_{p,init}$ case, $\widetilde{EC}_a$ and $\widetilde{EC}_e$ increase with d when $d < 100$ cm, decrease with d between 100 cm $< d <$ 150 cm, and remain almost constant with $d >$ 150 cm (Fig. 11b). Thus, for observing salt accumulation in the field, a measurement as close as possible to dripline will capture the largest portion of EC_a and EC_e for the low $EC_{p,init}$ case, and a measurement at $d \sim 100$ cm will be optimal for the high $EC_{p,init}$ case. The high $EC_{p,init}$ case for $\widetilde{EC}_a$ down to the 75 cm depth has a large variability for small d values indicating that some of the ensemble members may have the highest $\widetilde{EC}_a$ in that area. This is also suggested by the low correlation and high variability of EC_a at a 75 cm depth shown in Fig. 8,d,f.

Other case studies can result in different results and present a different optimal location for measurements. Moreover, more considerations may be involved in choosing the optimal d, such as the desire to measure in an active root-zone area where the measured salinity is affecting the tree, or the desire to measure in an area that represents mean values rather than the highest salinity values.

4. Conclusions

Electromagnetic induction (EMI) measurements of soil electrical conductivity (EC_a) are routinely used to map and monitor soil salinity (EC_e). However, in drip-irrigated fields, EMI measurements are affected by the positioning of the instrument relative to drip emitters, potentially limiting their utility in determining EC_e. In this work, simulation was used to investigate optimal EMI measurement practices for drip irrigated systems. An ensemble modeling approach accounted for unknown or uncertain model parameters and inputs. Two case studies were developed, one with high initial soil salinity and low salinity irrigation water, and one with low initial soil salinity and high salinity irrigation water.

The ensemble simulations identified measurement positions where the correlation between EC_a and EC_e was high, as needed to reliably predict EC_e from EC_a. Analyses of the case studies found that reliable salinity monitoring was possible using proximal electrical conductivity measurements taken 80–150 cm from the emitter in the low initial soil salinity case, and 130–180 cm for the high initial soil salinity case. For the low initial salinity case, a measurement adjacent to the emitter was also reliable for detecting profile salinity down to a depth of 150 cm. Overall, the optimal measurement position for determining EC_a and EC_e was found to be directly adjacent to the emitter in the low initial soil salinity case, and 100 cm from the emitter in the high initial salinity case.

Many management, soil, and crop parameters are unknown. Among parameters considered uncertain in this study, irrigation water salinity and irrigation frequency had the largest effect on model ensemble

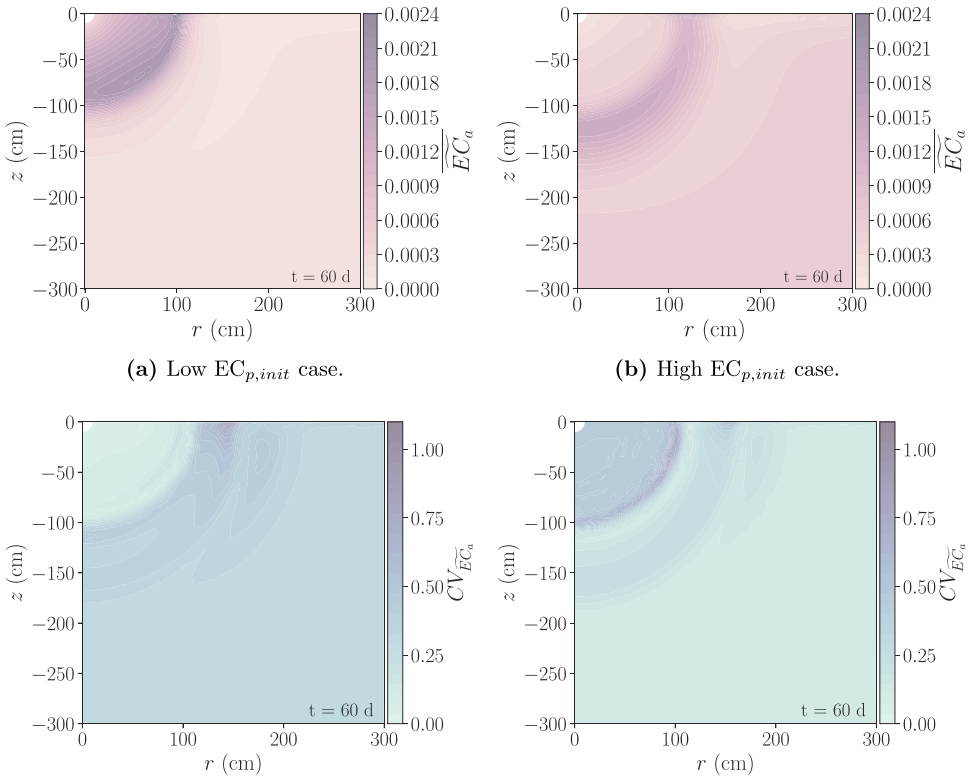

(a) Low $EC_{p,init}$ case. (b) High $EC_{p,init}$ case.

(c) Low $EC_{p,init}$ case. (d) High $EC_{p,init}$ case.

Fig. 9. Mean of normalized apparent EC ($\widetilde{EC}_a$) and the coefficient of variation (CV) of the normalized apparent EC ($\widetilde{EC}_a$) of the model ensemble at the end of the simulations.

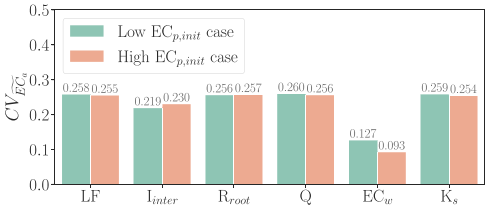

Fig. 10. Domain nodal mean of the apparent EC (EC_a) coefficient of variation (CV) of the ensemble, when each parameter is held fixed at its mid-value. LF is the irrigation leaching fraction, R_{root} is the root volume radius, Q is the emitter discharge, EC_w is the irrigation water electrical conductivity and K_s is the saturated hydraulic conductivity.

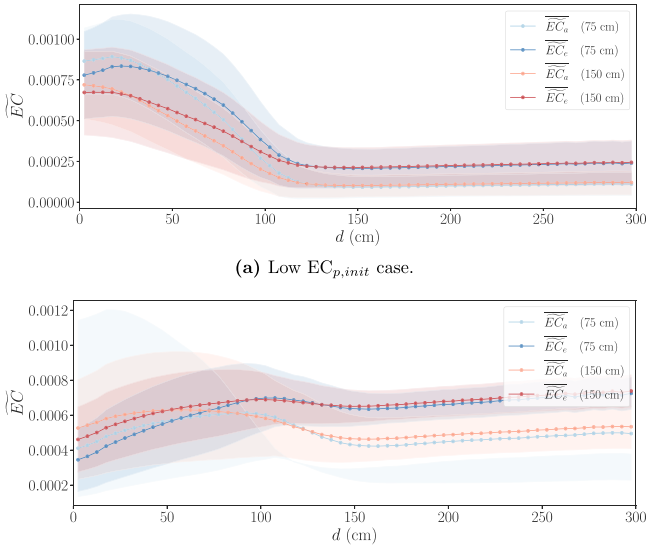

(a) Low $EC_{p,init}$ case.

(b) High $EC_{p,init}$ case.

Fig. 11. The mean of the normalized EC_e ($\widetilde{EC}_e$) and normalized EC_a ($\widetilde{EC}_a$) with distance from the drip-line (d), when traversing parallel to the drip-line (as illustrated on Fig. 5). Shaded regions show plus-or-minus two ensemble standard deviations.

variance. Thus, irrigation water quality and irrigation frequency were key factors in predicting soil solute distributions and in assessing optimal EC_a measurement locations.

The results obtained here are specific to the two considered case studies. At present, determining optimal measurement positioning for other irrigation scenarios would require applying the ensemble approach using parameters and inputs specific to each scenario. To simplify that process, future work aimed at identifying the most important parameters to include as part of the ensemble uncertainty analysis is needed. Additional parameters to consider could include the unsaturated soil hydraulic parameters. Through analyses of a wide range of additional scenarios, it may become possible to identify general recommendations for EMI-based measurements which could be applied when site-specific simulation analyses are not possible.

Declaration of Competing Interest

The authors declare that they have no known competing financial

interests or personal relationships that could have appeared to influence the work reported in this paper.

Data availability

Data will be made available on request.

Acknowledgments

We gratefully acknowledge the National Institute of Food and Agriculture (NIFA) for funding of the project - Agricultural Salinity Management via an Integration of Proximal and Remote Sensing with Big Geodata Modeling (Grant Number: 2019–67022-29696).

References

Allen, R.G., Pereira, L.S., Raes, D., Smith, M., et al., 1998. Crop Evapotranspiration-Guidelines for Computing Crop Water Requirements-fao Irrigation and Drainage Paper 56. FAO, Rome (300, D05109). http://www.avwatermaster.org/filingdocs/195/70653/172618e_5xAGWAx8.pdf.

Baram, S., Couvreur, V., Harter, T., Read, M., Brown, P., Hopmans, J., Smart, D., 2016. Assessment of orchard n losses to groundwater with a vadose zone monitoring network. Agric. Water Manag. 172, 83–95.

Bear, J., 2013. Dynamics of Fluids in Porous Media. Courier Corporation.

Burt, C.M., Isbell, B., 2005. Leaching of accumulated soil salinity under drip irrigation. Trans. ASAE 48, 2115–2121. https://doi.org/10.13031/2013.20097.

Burt, C.M., Isbell, B., Burt, L., 2003. Long-term salinity buildup on drip/micro irrigated trees in california. In: Proceedings of the Irrigation Association Techincal Conference, pp. 46–56.

Celia, M.A., Bouloutas, E.T., Zarba, R.L., 1990. A general mass-conservative numerical solution for the unsaturated flow equation. Water Resour. Res. 26, 1483–1496. https://doi.org/10.1029/wr026i007p01483.

Corwin, D., Lesch, S., 2003. Application of soil electrical conductivity to precision agriculture: theory, principles, and guidelines. Agron. J. 95, 455–471. https://doi.org/10.2134/agronj2003.4550.

Corwin, D., Lesch, S., 2005a. Apparent soil electrical conductivity measurements in agriculture. Comput. Electron. Agric. 46, 11–43. https://doi.org/10.1016/j.compag.2004.10.005.

Corwin, D., Lesch, S., 2005b. Characterizing soil spatial variability with apparent soil electrical conductivity: I. survey protocols. Comput. Electron. Agric. 46, 103–133. https://doi.org/10.1016/j.compag.2004.11.002.

Corwin, D., Scudiero, E., Zaccaria, D., 2022. Modified EC_a-EC_e protocols for mapping soil salinity under micro-irrigation. Agric. Water Manag. 269 https://doi.org/10.1016/j.agwat.2022.107640.

Corwin, D.L., Lesch, S.M., 2013. Protocols and guidelines for field-scale measurement of soil salinity distribution with eca-directed soil sampling. J. Environ. Eng. Geophys. 18, 1–25. https://doi.org/10.2113/jeeg18.1.1.

Corwin, D.L., Scudiero, E., 2020. Field-scale apparent soil electrical conductivity. Soil Sci. Soc. Am. J. 84, 1405–1441. https://doi.org/10.1002/saj2.20153.

Corwin, D.L., Yemoto, K., 2020. Salinity: Electrical conductivity and total dissolved solids. Soil Sci. Soc. Am. J. 84, 1442–1461. https://doi.org/10.1002/saj2.20154.

Dasberg, S., Or, D., 1999. Practical applications of drip irrigation. In: Drip Irrigation. Springer, pp. 125–138.

Farahani, H., Buchleiter, G., Brodahl, M., 2005. Characterization of apparent soil electrical conductivity variability in irrigated sandy and non-saline fields in colorado. Trans. ASAE 48, 155–168. https://doi.org/10.13031/2013.17959.

Feddes, R., Zaradny, H., 1978. Model for simulating soil-water content considering evapotranspiration-?comments. J. Hydrol. 37, 393–397. https://doi.org/10.1016/0022-1694(78)90030-6.

Goldhamer, D.A., 2005.Tree water requirements and regulated deficit irrigation. https://ucanr.edu/sites/fruitandnut/files/73693.pdf.

Grieve, C.M., Grattan, S.R., Maas, E.V., 2012. ASCE Manual and Reports on Engineering Practice No. 71 Agricultural Salinity Assessment and Management. 2nd ed. ASCE, pp. 405–459. Reston, VA. chapter 13 Plant salt tolerance. 71. ⟨https://www.ars.usda.gov/ARSUserFiles/20360500/pdf_pubs/P2246.pdf⟩. Reston, VA. chapter 13 Plant salt tolerance. 71.

Hengl, T., Mendes de Jesus, J., Heuvelink, G.B., Ruiperez Gonzalez, M., Kilibarda, M., Blagotić, A., Shangguan, W., Wright, M.N., Geng, X., Bauer-Marschallinger, B., et al., 2017. Soilgrids250m: Global gridded soil information based on machine learning. PLOS One 12, e0169748. https://doi.org/10.1371/journal.pone.0169748.

Kandelous, M.M., Šimunek, J., Van Genuchten, M.T., Malek, K., 2011. Soil water content distributions between two emitters of a subsurface drip irrigation system. Soil Sci. Soc. Am. J. 75, 488–497. https://doi.org/10.2136/sssaj2010.0181.

Kool, D., Agam, N., Lazarovitch, N., Heitman, J., Sauer, T., Ben-Gal, A., 2014. A review of approaches for evapotranspiration partitioning. Agric. For. Meteorol. 184, 56–70. https://doi.org/10.1016/j.agrformet.2013.09.003.

Lesch, S.M., Strauss, D.J., Rhoades, J.D., 1995. Spatial prediction of soil salinity using electromagnetic induction techniques: 1. statistical prediction models: a comparison of multiple linear regression and cokriging. Water Resour. Res. 31, 373–386. https://doi.org/10.1029/94wr02179.

Mehdi-Tounsi, H., Chelli-Chaabouni, A., Mahjoub-Boujnah, D., Boukhris, M., 2017. Long-term field response of pistachio to irrigation water salinity. Agric. Water Manag. 185, 1–12.

Mmolawa, K., Or, D., 2000. Root zone solute dynamics under drip irrigation: a review. Plant Soil 222, 163–190.

Pedrera-Parrilla, A., Van De Vijver, E., Van Meirvenne, M., Espejo-Pérez, A., Giráldez, J. V., Vanderlinden, K., 2016. Apparent electrical conductivity measurements in an olive orchard under wet and dry soil conditions: significance for clay and soil water content mapping. Precis. Agric. 17, 531–545. https://doi.org/10.1007/s11119-016-9435-z.

Rhoades, J., Manteghi, N., Shouse, P., Alves, W., 1989. Soil electrical conductivity and soil salinity: New formulations and calibrations. Soil Sci. Soc. Am. J. 53, 433–439. https://doi.org/10.2136/sssaj1989.03615995005300020020x.

Rhoades, J.D., Corwin, D.L., Lesch, S.M., 1999. Geospatial measurements of soil electrical conductivity to assess soil salinity and diffuse salt loading from irrigation. Geophys. Monogr. Am. Geophys. Union 108, 197–216. https://doi.org/10.1029/gm108p0197.

Rhoades, J., 1996. Salinity: Electrical conductivity and total dissolved solids.Methods of soil analysis: Part 3 chemical methods 5, 417–435.

Rhoades, J., Loveday, J., et al., 1990. Irrigation of Agricultural Crops. Monograph, American Society of Agronomists, Madison. chapter Salinity in Irrigated Agriculture. 30, 1089–1142.

Šimunek, J., Hopmans, J.W., 2009. Modeling compensated root water and nutrient uptake. Ecol. Model. 220, 505–521. https://doi.org/10.1016/j.ecolmodel.2008.11.004.

Van Genuchten, M.T., 1980. A closed-form equation for predicting the hydraulic conductivity of unsaturated soils. Soil Sci. Soc. Am. J. 44, 892–898. https://doi.org/10.2136/sssaj1980.03615995004400050002x.

Williams, B.G., Baker, G., 1982. An electromagnetic induction technique for reconnaissance surveys of soil salinity hazards. Soil Res. 20, 107–118. https://doi.org/10.1071/sr9820107.

Willmott, C.J., 1981. On the validation of models. Phys. Geogr. 2, 184–194. https://doi.org/10.1080/02723646.1981.10642213.

Zhang, Y., Schaap, M.G., 2017. Weighted recalibration of the rosetta pedotransfer model with improved estimates of hydraulic parameter distributions and summary statistics (rosetta3). J. Hydrol. 547, 39–53. https://doi.org/10.1016/j.jhydrol.2017.01.004.